ACS APPLIED MATERIALS & INTERFACES

Research Article

www.acsami.org

Transparent, Superhydrophobic Surface with Varied Surface Tension Responsiveness in Wettability Based on Tunable Porous Silica Structure for Gauging Liquid Surface Tension

Yan Wang,[†,‡] Yingjie Zhu,[†] Chunyang Zhang,[†,‡] Jun Li,[†,‡] and Zisheng Guan*[,†,‡]

[†]College of Materials Science and Engineering, Nanjing Tech University, Nanjing, Jiangsu 210009, China

[‡]Jiangsu Collaborative Innovation Center for Advanced Inorganic Function Composites, Nanjing 210009, China

Supporting Information

ABSTRACT: Any solid surface can spontaneously exhibit variational wettability toward liquids with varied surface tension (γ). However, this correspondence has seldom been proposed or used on an artificial superhydrophobic surface, which should be more remarkable and peculiar. Herein, we fabricated robust, transparent superhydrophobic surfaces utilizing acid- and base-catalyzed silica (AC- and BC-silica) particles combined with candle soot template for structural construction and the CVD process for chemical modification. Three types of porous silica structures were devised, which presented distinctive surface tension responsiveness in wettability. Interestingly, all types of surfaces (i.e., AC-, AC/BC-, and BC-silica) show high repellence to high surface tension liquid (γ > 35 mN/m), and small differences are observed. With decreasing γ of the ethanol−water mixtures (γ < 35 mN/m), the static contact angles (SCAs) on all surfaces have an evident decline, but the features of the decreases are fairly different. As γ decreases, the SCA on the AC-silica surface decreases gradually, but the extent of decline becomes larger when γ < 27.42 mN/m. However, the SCA on the BC-silica surface decreases gradually except for $\gamma \approx$ 30.81 mN/m, and the SCA undergoes a sharp decline at $\gamma \approx$ 30.81 mN/m. The SCA on the AC/BC-silica surface has a similar variation as that of the SCA on the BC-silica surface, but a lower rate of BC-silica particles, e.g., 1/16, 1/8, 1/1 (AC/BC), further diminishes the critical γ values (where a sharp SCA drop occurs) to 30.16, 29.56, and 28.04 mN/m, respectively. The diversity is believed to be ascribed to the structure-induced selectivity of pore infiltration for the liquid. The tunable responsiveness can be generalized to various classes of organic aqueous solutions including methanol, acetic acid, acetone, and *N*,*N*-dimethylformamide. Benefiting from this, we can estimate organics concentration of an organic aqueous solution as well as its liquid surface tension by detecting its wettability on all of the diverse superhydrophobic surfaces.

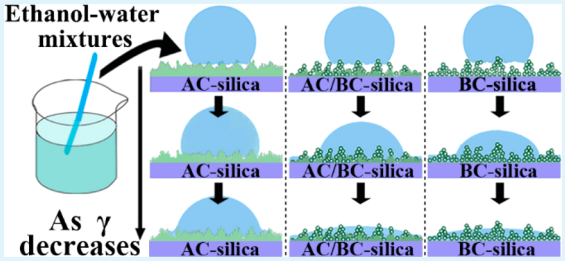

KEYWORDS: *surface tension responsive, superhydrophobic, transparent, sol−gel, porous silica*

1. INTRODUCTION

Abundant nonadhesive surfaces with opportune texturing, motivated by commonly observed natural organisms covering lotus leaves, duck feathers, and water striders, have been framed to address technological and scientific issues on the basis of their enormous potentials in self-cleaning, antifouling, antifogging, antibacterial, and optical applications.[1−6] Given the synergic effects of hierarchically structured topography and low surface energy materials, these artificial surfaces are endowed with large water contact angles (WCAs > 150°) and low sliding angles (SAs < 10°).[7,8] Recently, it has been reported that some man-made surfaces can respond to external stimuli such as pH, temperature, light irradiation, and different types of solvents.[9,10] Using stimuli-responsive hydrogels as the main raw material, Huang et al.[11] fabricated surfaces that can reversibly vary from superhydrophobicity to superhydrophilicity under the influence of an external stimulus, including pH, temperature, and stress. Burgess et al.[12] reported a surface with fluid-specific optical response in a three-dimensional photonic crystal. Nevertheless, among these responsive materials, the responsiveness derived from varied hybrid liquids with controllable surface tension was seldom proposed. The contact angles of ethanol−water mixtures (0−100% by ethanol volume fraction) have recently been investigated on a rough polydimethylsiloxane (PDMS) surface in comparison with a planar PDMS surface, which disclosed the conclusive effect of surface texturing on the wetting scenario.[13] These prepared surfaces, not pertaining to the genuine superhydrophobic scope however, cannot facilitate the detection of wettability response toward the diversity of an extremely coarse surface. Inspired by superhydrophobic porous nanostructure models with tunable water adhesion,[14] we can regulate diverse porous nanostructures to fabricate surfaces with different surface-tension

Received: October 9, 2016
Accepted: January 10, 2017
Published: January 10, 2017

DOI: 10.1021/acsami.6b12779
ACS Appl. Mater. Interfaces 2017, 9, 4142−4150

responsiveness and then estimate the surface tension of a liquid solution.

The surface tension of a liquid can be approximately measured by several conventional techniques (e.g., testing the interfacial energies between the liquid and a solid object, probing resonant oscillations of liquid dropping, using a maximum bubble pressure method, and so on). Recently, Wang et al.[15] developed a novel one-way oil-transport ZnO/POSS-coated fabric that was capable of estimating the surface tension of an ethanol−water mixture simply by observing the transport features on a series of fabrics. Because a wide range of the surface tension values is obtained by this method, more novel and accurate methods to gauge surface tension are expected. It has been demonstrated that, with increasing ethanol concentration, the surface tension value of an ethanol−water mixture decreases in the range of 72.75−22.31 mN/m (at 20 °C).[16] When these various liquid solutions are dropped on a nonwetting surface (with the surface energy much less than 72.75 mN/m), the exhibited SCAs will range from high to low depending on the liquid concentration (or surface tension). However, utilizing wetting responsiveness on diverse superhydrophobic coarse structures to estimate the liquid surface tension has not yet been reported. Hence, it will make sense to propose such a smart surface to spontaneously gauge liquid surface tension and further estimate liquid concentration.

For such superhydrophobic surfaces to be obtained, the sol−gel method can be employed as an ideal candidate because it can generate silica spheres or linear silica particles to provide coarse structure.[17] By blending two types of silica at different ratios, it is facile to control the surface morphologies.[17,18] Aside from structure adjustment, high transmittance and abrasion-resistant properties are other important factors to consider if we want to expand their applications.[19,20] Recent progress in fabricating multifunctional superhydrophobic coatings (made by our group[21−23]) revealed that the candle-soot template is a good approach to increase roughness, and CVD of PDMS for modification can lower the coating surface energy. Herein, utilizing a silica-based sol−gel process combined with templating method and CVD modification, we fabricated superhydrophobic surfaces with ideal porous structures that can simultaneously impart favorable transparency, excellent robustness, and the most significant surface tension responsiveness. Aiming to create tunable surface tension responsiveness, we devised three types of superhydrophobic nanostructures including AC-, BC-, AC/BC-silica. We found that the SCAs of liquid solutions on the surface had a positive correlation with liquid surface tension. Meanwhile, varied porous structures had apparent influences on the wetting behaviors of liquid solutions. The liquid solutions were extended into organic aqueous solutions including methanol, ethanol, acetic acid, acetone, *N*,*N*-dimethylformamide (DMF), etc. We further disclosed that the surface could be employed as an effective test for liquid concentration (or liquid surface tension) of a typical liquid solution. This work can provide new thinking for a multifunctional superhydrophobic surface.

2. EXPERIMENTAL SECTION

2.1. Materials. Adopted as substrates, 7101 slides (25.4 mm × 76 mm × 1.2 mm) with an original WCA of 10 ± 2.5° were purchased from the market. Commercially used paraffin wax and cotton threads were obtained from the market to prepare candles. *N*,*N*-Dimethylformamide (DMF, 99.5%), acetic acid (99.5%), tetraethyl orthosilicate (TEOS, 98%), methyltriethoxysilane (98%), aqueous ammonia ($NH_3{\cdot}H_2O$, 25%), hydrochloric acid (HCl, 37%), and absolute ethanol (99.5%) were obtained from Sinopharm Chemical. High purity water with a resistivity of 18.25 MΩ cm^{-1} was employed in the experiment, and fluid Sylgard 107 (*α*,*ω*-dihydroxypolydimethylsiloxane) with a viscosity of 5000 cps was purchased from Jiangxi Xinghuo Organic Silicone Plant (China). Dibutyltindilaurate (DBTDL, 97%), methanol (99.5%), acetone (99.5%), isopropanol (99.5%), and propyl alcohol (99.5%) were received from Shanghai Lingfeng Chemical Reagent Co., Ltd. (China). All laboratory supplies were used as received.

2.2. Preparation of Diverse Silica Solutions. In the acid-catalyzed sol−gel (AC Sol) process, TEOS, HCl, H_2O, and absolute ethanol were mixed at a molar ratio of 1:0.06:4:37. After magnetic stirring for 1 h, the mixture was left at room temperature for 3 days. Accordingly, silica colloid particles with an average diameter of approximately 5−10 nm were attained. When preparing base-catalyzed sol (BC sol), an ammonia ethanol solution was added dropwise into TEOS in the absolute ethanol. After the addition of deionized water, the mixture was continuously stirred for 1 h and spontaneously aged for 3 days. The final molar ratio of TEOS/$NH_3{\cdot}H_2O$/H_2O/absolute ethanol was 1:0.8:1.2:37. Subsequently, a slightly whitish silica solution, namely BC Sol, was formed at room temperature. For the sake of stability of the resulting silica particles, the above sols were agitated in a ventilating cabinet to remove ammonia and hydrochloric acid. With the removal of hydrolysis catalyzer, AC Sol and BC Sol were mixed at mass ratios of 2:1, 1:1, 1:8, and 1:16 (the content of BC sol was 33.33, 50, 88.89, and 94%, respectively) under magnetic stirring for 30 min to produce different acid−base-catalyzed hybrid silica solutions (collectively called AC/BC Sol).

2.3. Creation of Transparent Superhydrophobic Surfaces. Glass slides were first cleaned by an overnight immersion in absolute ethanol, entirely dried at 60 °C, and then promptly moved back and forth through the middle of the candle flame until the slides turned wholly black. After respective dip-coating in AC Sol, BC Sol, or AC/BC Sol at a speed of 1 mm/s, the glass slides were directly subjected to the calefaction procedure in a muffle furnace with a heating speed of 5 °C/min and a holding time of 1 h in air at 550 °C. Subsequently, stable, rough, and superhydrophilic silica coatings appeared on the glass slides. The fluid Sylgard 107, methyltriethoxysilane, and DBTDL were mixed at a mass ratio of 50:10:1 and baked at 60 °C for 12 h to fabricate the cured PDMS. In a stainless steel container (10 cm × Φ10 cm) with a hole (Φ5 cm) on the cover, the superhydrophilic substrates were conducted by a CVD process in which 0.1 mg of PDMS was used and heated at 330 °C for 0.5 h. After the slides were naturally cooled to room temperature, the target coatings were obtained.

2.4. Characterization. Field-emission scanning electron microscopy (FE-SEM, Hitachi, S-4800) was used to detect surface morphologies of the as-prepared coatings. For the electrical conductivity to be improved, the samples were coated with a thin gold layer before being measured. WCA and SA were measured using 5 and 12.5 μL deionized water droplets, respectively, which were conducted in three different positions of the samples on a commercial contact-angle meter (JC2000CS) equipped with a CCD camera. Moreover, the SCA in the ethanol−water studies was measured using 12.5 μL mixture droplets. Transmittance measurements were performed on a UV−vis−NIR spectrophotometer (UV-3600, SHIMADZU).

3. RESULTS AND DISCUSSION

Figure 1a demonstrates the forming process of hybrid SiO_2 nanoparticles. Silica particles can be synthesized by the sol−gel process involving the formation of silanol by primary hydrolysis and a multidimensional network of colloidal particles through water condensation reactions. The regulations of hydrolysis, catalyst effects, and condensation reactions are elaborated in the literature.[24] It is acknowledged that using aqueous ammonia and hydrochloric acid respectively as catalyst in the sol−gel method can yield diverse nanoscale silica colloid particles that

DOI: 10.1021/acsami.6b12779
ACS Appl. Mater. Interfaces 2017, 9, 4142−4150

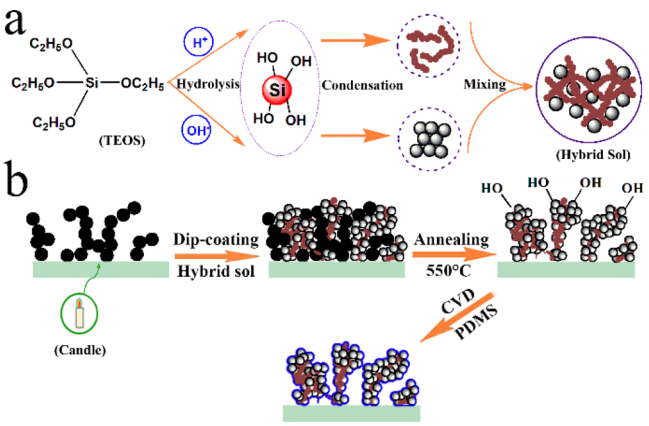

Figure 1. Schematic procedure for preparing the target superhydrophobic surfaces: (a) forming process of hybrid SiO_2 nanoparticles via sol−gel method and (b) structural construction and CVD modification.

exhibit different surface microstructures. Under acidic conditions, the silica particle growth or agglomeration holds until the particle size reaches approximately 5 nm, where the size-dependent solubility is greatly reduced. The resulting linear chain mostly composed of small primary particles was prepared. For the base-catalyzed sol−gel process, however, the formation of larger particles due to better solubility (above pH 7) generates the silica cluster and particulate sol. Then, blending polymeric chains with a particulate network could produce the hybrid silica sol where the larger spherical particles cluster around well-connected polymeric chains. Figure 1b schematically depicts the fabrication procedure of the superhydrophobic (hybrid silica) coating. First, candle soot was deposited on the glass substrates through the operation over the candle flame. The blended silica solution was then applied to the candle soot-coated glass through a dip-coating technique. The pores of the deposited candle soot gave space for the hybrid silica particles to penetrate in and attach to the substrates. Later, the coated glass was calcined at 550 °C to remove candle soot template, and then, vast nanosized pores formed on the superhydrophilic glass. During this period, some fusion, especially twining mode, may occur at 550 °C to the same kind of silica nanoparticles and even the diverse silica nanoparticles, thus enhancing the binding force between the adjacent particles as well as the mechanical strength of the coatings. Finally, the low surface energy substance was then applied to the above superhydrophilic glass by a novel CVD modification of cured PDMS, where PDMS successively experienced decomposition and oxidation at 330 °C.[21] As a main decomposition product, hexamethylcyclotrisiloxane (HMCTSO)[25] immediately experienced oxidation in air with the help of high temperature to modify the hydrophilic SiO_2 nanoparticles. Thus, the porous, stable, and superhydrophobic silica coating was formed due to the increased surface roughness and reduced surface energy.

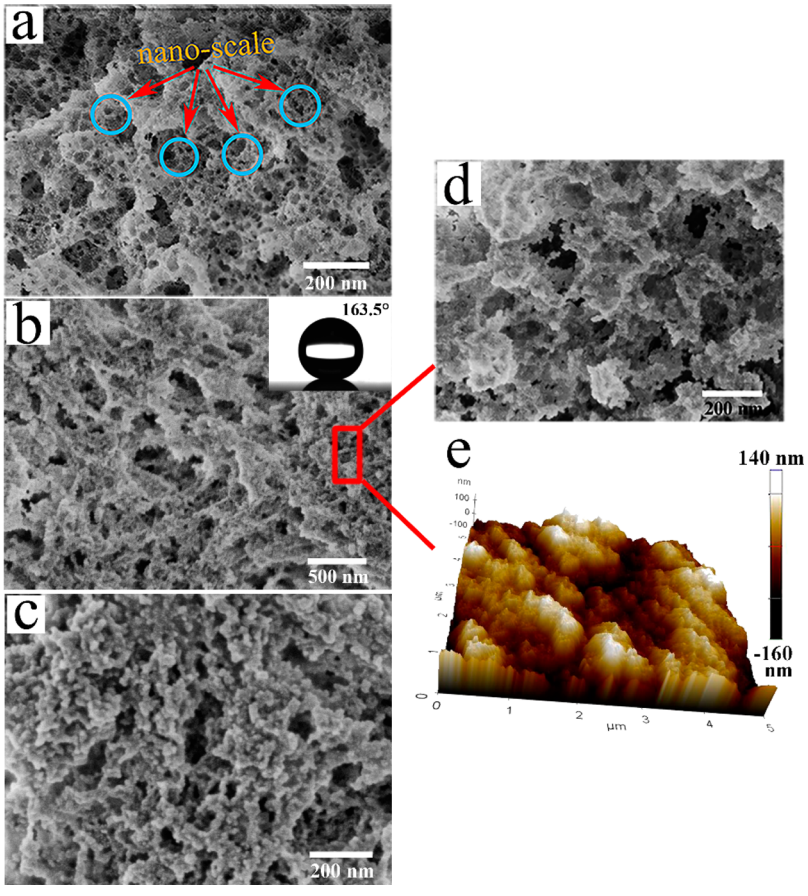

Figure 2. SEM images of the superhydrophobic surface prepared using (a) AC-silica particles, (b) blended silica particles (target surface as 1:8), and (c) BC-silica particles. (d) Partial magnification of (b). (e) Corresponding AFM images of target surface (b,d). Blue circles in (a) indicate nanoscale pores.

DOI: 10.1021/acsami.6b12779
ACS Appl. Mater. Interfaces 2017, 9, 4142−4150

Figure 2a shows that the AC-silica superhydrophobic coating is covered by dense silica network where plenty of nanoscale concave pits were formed along with several submicrometer-scale pores. The concave pits were around 10−20 nm in diameter and randomly distributed to coating, thus constituting a honeycomb-like morphology. As revealed in Figure 2b, the modified AC/BC (1:8)-blended silica particle layer possessed a rough concave-convex structure. In the BC-silica layer, massive spherical silica nanoparticles accumulated on the glass substrate and were interconnected, forming a multidimensional morphology (Figure 2c). Furthermore, the mean particle sizes shifted to larger values, and many submicrometer-scale pores were still observed in this porous and coarse surface, which was devoid of nanosized pits. Intrinsically, utilizing a well-interlinked AC/BC-silica network, thus generating hybrid chain/sphere structure, obviously caused a loss of nanosized concave pits owing to the filling of silica spheres and low rates of chain particles (Figure 2d, e). With the increase in BC-silica particle rate, there was a corresponding increase in convex cluster structures but an evident decline in particle coverage rates (see the Supporting Information). Thus, by controlling the ratio of AC- to BC-silica, it is fairly novel and facile to obtain superhydrophobicity with varied surface structural topographies.

As evidenced by the UV/vis transmittance spectra in Figure 3a, these coarse nanostructures have slight effects on the transparency of silica coatings. The average transmittances (ATs) at visible wavelengths (400−800 nm) were 58.48 and 82.61% for AC- and AC/BC-silica coatings (the latter obtained by mixing AC/BC Sol at a ratio of 1:8), respectively. The BC-silica coating showed 85.19% AT within the visible range, close to the performance of the bare glass slide. Notably, there was a distinct improvement for AT with an increasing amount of BC-silica particles. The results revealed that the incorporation of porous BC-silica entitled the coating with enhanced transparency due to their higher porosity and lower refractive index.[26,27] Favorable transparency can be more directly reflected by the distinct letter beneath the sample of AC/BC-silica (1:8) coating; its high superhydrophobicity is indicated by the nearly spherical state of many randomly distributed liquid droplets (including milk, coffee, purple vodka, strawberry juice, and water) on such a transparent coating (Figure 3b).

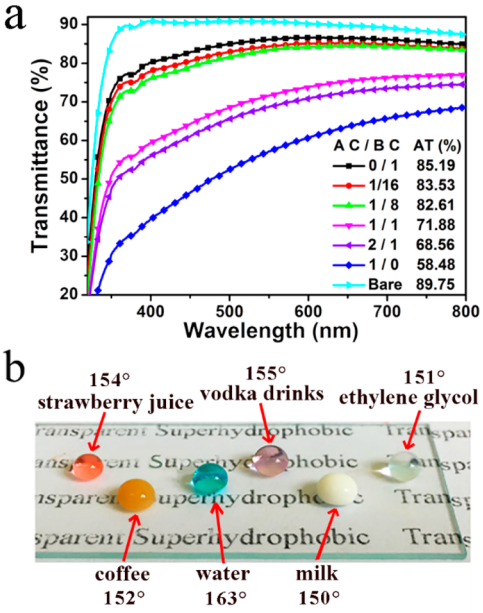

Figure 3. Transmittance and superhydrophobicity of the coatings. (a) Transmittance of the superhydrophobic coatings obtained from silica particles with different blended ratios. (b) Photographs of deposited liquid mixture droplets (10 μL for each volume) and water drops (10 μL) on such a transparent coating.

For the influence of surface microstructure on the coating durability to be investigated, a series of tests were carried out, including water-droplet impingement test,[28] solution immersion experiment, and thermal stability test (see details in the Supporting Information). It is observed that, as the rate of BC-silica increases, the total volume of impacted water damaging the superhydrophobicity undergoes an increase to 20 L followed by a decrease to 12 L (Figure 4a). As outlined in Figure S4a, the twining mode and particle fusion, instead of a weak physical bond, enhanced the particle−particle bonding due to introduction of BC-silica,[17] which was in agreement with our results. However, induced by further augmentation of BC-silica nanoparticles, less and weaker linkages between individual particles lower the coating strength. Given the best resistance to water-droplet impacting, the AC/BC-silica (1/8) coating was selected as target coating (henceforth referred to AC/BC-silica coating) for further testing of the coating stability.

For the target coating, a WCA higher than 160° and an SA less than 2° occurred therein after 15 L water impacting (4×10^5 drops), and the coating retained its nonadhesive superhydrophobicity (with WCA higher than 150°) even after 19.5 L water impacting (Figure 4b). The WCA was as high as 147.5° ± 1° even if the surface was abraded by 20 L water impacting. There were little changes for the WCA and SA of the immersed coating in the neutral solution within a week, indicating good stability (see data in Figure 4c). However, with extended immersion time, the WCA decreased and remained stable close to 152° after 17 days. As for the coatings immersed in the acidic and basic solutions, they maintained superhydrophobicity for approximately 6 days and 12 h, respectively, and their WCAs were stable near 135° and 20° after 17 days of immersion. The significant effects of acidic and basic solutions on the coating can be explained by the cumulative corrosive reactions including hydrolyzation and remodeling of micronano structures.[29] Thorough destruction of rough structures happened in the base-immersed coating, whereas few changes occurred to the morphology for acid- and neutral-immersed coatings, which could be further demonstrated by the WCAs of the immersed examples after re-CVD (Supporting Information). As shown in Figure 4d, WCAs and SAs of the coating were stable below 420 °C, and the surface remained superhydrophobic with a slightly smaller WCA (150°) after the temperature further increased to 440 °C, indicating good thermal stability of the as-fabricated coating. However, further increasing the temperature (460 °C or higher) led to loss of superhydrophobicity owing to the thermal oxidization of the silyl groups. The destroyed coating regained superhydrophobicity and nonadhesion after re-CVD of PDMS, which was due to the preserved nanosized rough structures (see the SEM image in Figure S4c).

Table 1 presents the dependence of WCA and SA on the coating composition, which indicates that the superhydrophobicity of the as-prepared samples is not apparently changed by mixing AC Sol and BC Sol at different ratios. All WCAs measured for these silica coatings are more than 161°, and SAs for them are less than 3°. This evidence suggests that all samples display nonadhesiveness and that the different

DOI: 10.1021/acsami.6b12779
ACS Appl. Mater. Interfaces 2017, 9, 4142−4150

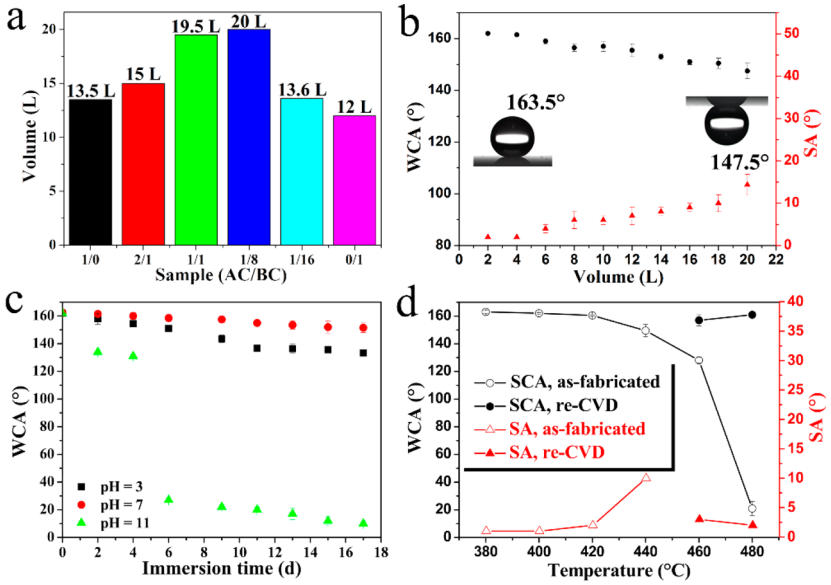

Figure 4. Robustness and durability of the superhydrophobic coating. (a) Water volumes to damage the as-fabricated coatings. (b) Dependence of WCAs and SAs of the target surface on the water-drop impinge volumes. (c) pH and the immersion time dependence of WCAs for the target superhydrophobic coating. (d) WCAs and SAs after thermal-treated coatings for 1 h at a series of temperatures.

Table 1. Wettability of the Superhydrophobic AC/BC Blended Silica Coatings Prepared with Varied Mass Proportions of AC Sol to BC Sol

AC/BC	1:0	2:1	1:1	1:8	1:16	0:1
WCA/deg	162.0 ± 1.0	163.0 ± 1.0	163.0 ± 0.5	163.5 ± 0.5	164.0 ± 1.0	164.0 ± 0.5
SA/deg	2.0 ± 0.5	2.0 ± 0.5	2.0 ± 0.5	1.0 ± 0.5	1.0 ± 0.5	1.0 ± 0.5

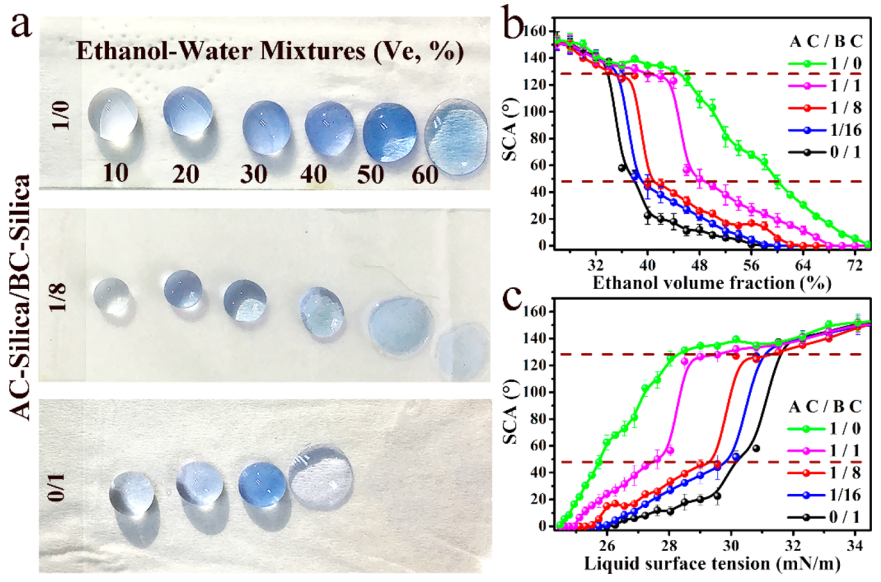

Figure 5. (a) Photos of ethanol−water droplets with different ethanol concentrations on the AC-silica (1:0) coating, BC-silica (0:1) coating, and AC/BC-silica (1:8) coating. (b) SCAs of ethanol−water mixtures with different volume concentrations on all types of superhydrophobic coatings. (c) Dependence of SCAs of all porous coatings on the mixtures' liquid surface tension as calculated from the theoretical model.

morphologies do not apparently affect their wettability to pure water. However, many differences may appear when it comes to the liquid with lower surface tension.

It has been demonstrated that the surface tension value of an ethanol−water mixture decreases in the range of 72.75−22.31 mN/m (at 25 °C) with increasing ethanol concentration.[16] Thus, a series of ethanol−water mixtures with different ethanol volume concentrations (V_e) were utilized to detect the variation of the SCAs on the porous superhydrophobic surfaces.

Figure 5a shows the wetting features of ethanol−water mixtures that are different on three types of coatings. With increasing V_e, the wettability of ethanol−water mixtures on the AC-silica surface increased gradually, but that on the other two coatings sharply changed from nonwetting to wetting in the range of 30−40%. The lowest V_e of mixture drops to wetting

DOI: 10.1021/acsami.6b12779
ACS Appl. Mater. Interfaces 2017, 9, 4142−4150

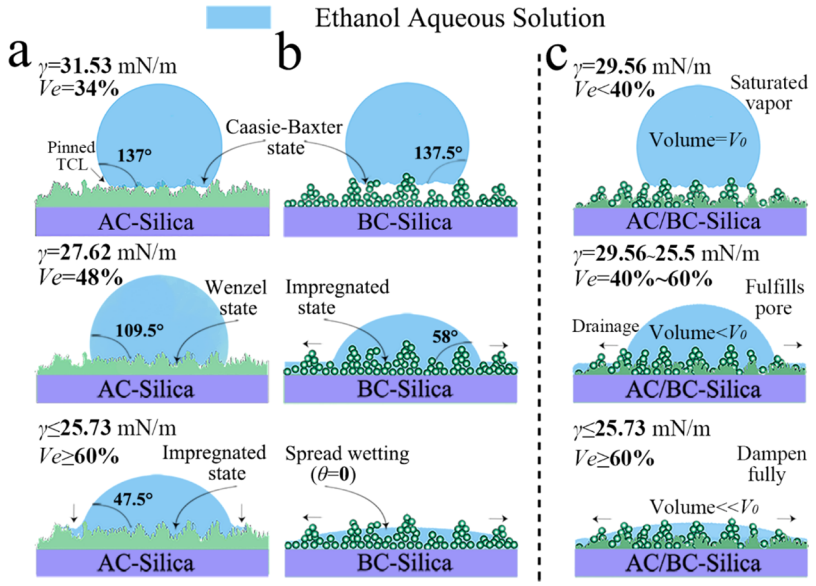

Figure 6. Illustration of the decrease in the contact angles of ethanol−water mixtures with increasing ethanol concentration on various superhyphobic surfaces including (a) AC-, (b) BC-, and (c) AC/BC-silica (1:8) surfaces. The difference of wetting behavior on the AC- and BC-silica surfaces is shown left of the dotted line. As illustrated right of the dotted line, the scenario in the AC/BC-silica resembles the BC-silica surface, although some differences appear in the turning points.

the AC-silica surface was obviously higher than that to wetting the other two surfaces. All coatings can show super-repellency to mixtures with V_e lower than 28% (see data in the Supporting Information), but it changed dramatically when V_e exceeded 28%. As revealed in Figure 5b, the AC-silica coating was repellent to the ethanol−water mixtures with V_e less than 46%, whereas the repellency decreased gradually with increasing V_e ($V_e \geq 48\%$). The lowest V_e of the mixture to fully wetting the AC-silica coating increased to 74%. For the BC-silica superhydrophobic coating, the SCA gradually decreased to 137° up to $V_e \approx 34\%$ and then sharply decreased to 58° when V_e increased to 36%. After $V_e \geq 36\%$, SCA gradually decreased until $V_e \approx 60\%$. Note that the SCA variation on the AC/BC-silica coating resembles that on the BC-silica coating. However, a lower rate of BC particles, e.g., 1:16, 1:8, and 1:1 (AC/BC), further extended the lowest V_e of mixture drops to wetting the surface to 38, 40, and 46%, respectively. For example, a sharp decrease of SCA on the AC/BC-silica (1:8) coating occurred at a higher V_e range (38−40%), and the SCA of mixtures decreased gradually in the range of 46.5°−0° after $V_e \geq 40\%$. Notably, with the increasing BC-silica particles of porous coating, its repellency to ethanol−water mixtures with V_e exceeding 36% was reduced.

The ethanol concentration in water has a negative correlation with the liquid surface tension (Supporting Information). By employing the nonlinear least-squares curve fitting combined with the shishkowski model,[30] the relevance between V_e and surface tension (γ) can be clarified. The code of the curve fitting is characterized as

$$\gamma = 11.11e^{-(V_e/2.23)} + 37.80e^{-(V_e/22.80)} + 23.02 \quad (1)$$

The values of surface tension for all required ethanol aqueous solutions could be calculated using this equation. Thus, we can correlate the SCAs of ethanol aqueous solutions with their surface tension. We noted that no obvious variation in SCA occurs on the surfaces until γ decreases to 35 mN/m (Supporting Information). Figure 5c shows that SCAs on the surfaces change obviously in the γ range of 25−35 mN/m. As γ of the ethanol−water mixture decreased, its SCA on the AC-silica surface had a gradual decrease to $\gamma \approx 27.42$ mN/m and decreased dramatically after $\gamma < 27.42$ mN/m. The SCA on the BC-silica surface underwent a sharp decline with γ from 31.53 to 30.81 mN/m. Except for this γ range, the SCA decreased gradually. The scenario for all AC/BC-silica coatings resembled that of the BC-silica surface, but a sharp drop of SCA occurred at γ = 30.16, 29.56, and 28.04 mN/m for AC/BC-silica coating (1:16, 1:8, 1:1, respectively).

Figure 6 schematically correlates the wetting states of ethanol−water mixtures with the features of porous structures. After being dropped on three porous surfaces, droplets of ethanol−water mixtures (γ from 35 to 31.53 mN/m) were substantially suspended on the topsides of the cavities or concave pits instead of penetrating into the inside, indicating that it was in the Cassie state.[31] The SCA can be depicted as the equation[32] $\cos(\theta_c) = (1 - \varphi_v)\cos(\theta_0) - \varphi_v$, where θ_c, θ_0, and φ_v represent the Cassie SCA, intrinsic angle, and air fraction, respectively. Through this equation, the SCA of the mixtures decreases mainly because of the reduction of the intrinsic angle (local angle or θ_0) with increasing ethanol concentration. Because they are reported to be in a metastable state, the Cassie state of these superhydrophobic surfaces would break down when γ of the liquid droplets is under a critical value (henceforth referred to as the break-in point).[33] For the AC-silica coating, as shown in Figure 6a, the nanostructures were not penetrated by drops until γ was set at a low value (27.62 mN/m). As discussed earlier (Figure 2a), the AC-silica coating exhibited the closed nanosized groove structure, which would be expected to generate the approximate solid−liquid "line contact" behavior.[14] This behavior may pin the triple-phase contact line (TCL) at the topside of the porous structure and generate high air pockets so that it is hard for droplets to penetrate into the pores (Supporting Information). When the droplet was overhung on the topside of nanosized pores, the capillary force, Δp_r, can be calculated as $\Delta p_r = 2 \times \gamma/R$,[34,35] where R is the curvature radius of curved triple-phase lines.

DOI: 10.1021/acsami.6b12779
ACS Appl. Mater. Interfaces 2017, 9, 4142−4150

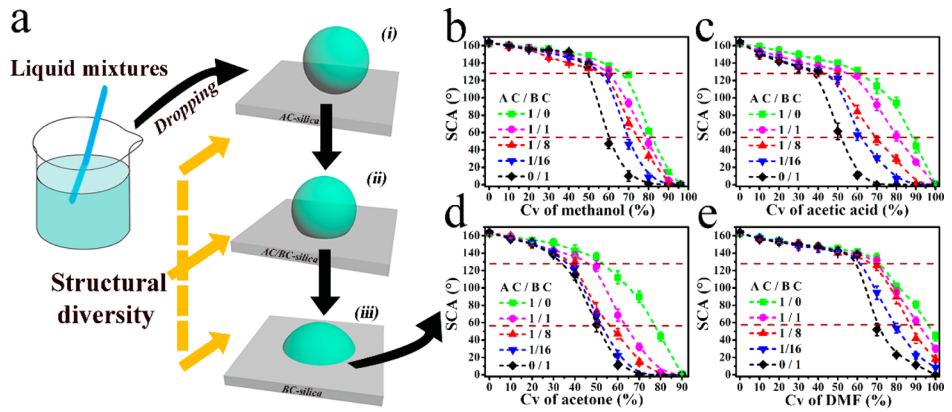

Figure 7. Surface tension responsiveness of superhydrophobic coating to various liquid solutions: (a) principles of gauging liquid surface tension; dependence of SCAs on the volume fraction of (b) methanol, (c) acetic acid, (d) acetone, and (e) DMF. C_v represents the liquid volume fraction.

There could be significantly higher Δp_r generated by a smaller R in the AC-silica coating compared to those of others. As the liquid surface tension decreased gradually, a lower γ could make the Δp_r of drops decrease to a critical point (below the molecular gravity), and then the γ at the break-in point was further lowered. After infiltrating into the pits, droplets cannot flow into the pores outside the contact area because of the closed groove system. Thus, the SCA decreased gradually with the decreasing γ and drops did not reach the Cassie-impregnated state until V_e exceeded 60% ($\gamma \leq 25.73$ mN/m). After the surface structure was impregnated by mixtures, the decreasing liquid tension reduced the intrinsic angle in correlation with the decrease of SCA. A mixture droplet with γ lower than 24.49 mN/m fully dampened the AC-silica surface.

For the BC-silica coating accompanied by the submicrometer convex structure (Figure 2c), coarse and sparse spherical particles or clusters generated the typical "point contact" behavior[36] with a smaller contact area and extremely discrete TCL. Thus, droplets with an appropriate γ can penetrate into the structure easily. For $\gamma = 30.81$ mN/m, the θ_0 of the mixture drops was less than 90°, and then the BC-silica surface was not able to hold back the penetration of the droplet (Figure 6b). Actually, the well-connected valleys between pores prompted the flow of intrusive liquids into the pores outside the contact area, and the transition to the Cassie-impregnated state[13] happened within 20 s (Supporting Information). Thus, a dramatic decrease in SCA occurred here. As the γ decreased to 26.25 mN/m, the pores outside the contact area were partially filled, and the surface was fully wetted by the mixture droplets—approaching the thermodynamic equilibrium. Figure 6c indicates that the wetting performance on the AC/BC-silica (1:8) surface resembles the performance on the BC-silica surface, but the transition to the Cassie-impregnated state appears at a lower γ (29.56 mN/m). Owing to coexistence of connected cavities structures and closed concave pits, the AC/BC-silica coating could be a little harder than BC-silica coating to penetrating into. So γ at the break-in point of AC/BC-silica coating was lowered. In general, the characteristics of porous structures are dominant to the diverse wetting responsibilities and only the AC-silica coating can display moderate γ-dependent SCA curves due to gradual pore penetration.

The procedure of gauging solute concentration in a liquid solution is illustrated schematically Figure 7a. When a liquid solution is respectively dropped on the three kinds of surfaces, they may display different SCAs. On the basis of the measured SCAs and the responsive curve, the liquid concentration (or the surface tension) can be available. Via fine-tuning of the blended ratio of AC- and BC-silica, different responsive curves can be obtained, leading to finer testing values. Taking ethanol as an example, we can estimate V_e (or γ) according to the almost linear dependence on the AC-silica surface and further reduce the error of V_e by analyzing wetting diversity of the other surfaces. Apart from ethanol, the system can be generalized to a series of commonly used organic solvents (that could be mixed with water at random ratios) including methanol, acetic acid, acetone, DMF, and so forth (Figure 7b–e and Supporting Information). The results show that the thresholds between the Cassie and Wenzel states for methanol, acetic acid, acetone, and DMF occur in the ranges of 50–70%, 40–60%, 30–50%, and 60–80%, respectively. Except for DMF, these pure solvents could fully wet the three superhydrophobic surfaces. Two notable properties are that, (i) when more BC-silica particles are mixed with AC-silica particles, all of the responsive curves present the responsiveness (from the liquid concentration) ranging from very moderate to very sensitive and the threshold (liquid concentration) between nonwetting and wetting states is reduced, and (ii) the threshold range between the Cassie and Wenzel state occurs at diverse concentrations for different liquids. For various classes of liquid mixtures with the same liquid volume fraction, the remarkable selectivity of infiltration on the porous structures may be attributed to the individual liquid surface tension. According to the responsive curve and the measured SCAs, the liquid concentration (or the surface tension) can be available. Beyond this, we foresee that this system will find use as an effective test for liquid surface tension as well as liquid concentration and also to determine the textural properties (including pore sizes, geometries, porosity, etc.) of the porous surface through the results of a liquid with known surface tension.

4. CONCLUSIONS

Utilizing the AC- and BC-silica composited particles incorporated with candle soot template for structural construction and CVD process for chemical modification, we proposed a novel and cost-effective approach to prepare a transparent, robust, superhydrophobic coating. The as-fabricated superhydrophobic coating displayed favorable resistance to high temperature (at most 440 °C), water, acidic solution, and at most 20 L drop-impinging. The results reveal that the SCAs of liquid solutions on the surface had a negative correlation with liquid

DOI: 10.1021/acsami.6b12779
ACS Appl. Mater. Interfaces 2017, 9, 4142–4150

concentration and a positive correlation with liquid surface tension. As the amount of BC-silica particles on the surface increased, the surface microstructures gradually ranged from closed concave pits to connected cavities. We disclosed that this structural variation had an apparent influence on the wetting response to the liquid surface tension. By measuring the SCAs of the mixture droplets on a series of diverse superhydrophobic coatings, their liquid surface tension could be estimated along with concentration. Thus, we anticipate that tunable surface tension-responsive surfaces will be used as an effective test for liquid surface tension as well as liquid concentration.

■ ASSOCIATED CONTENT

Supporting Information

The Supporting Information is available free of charge on the ACS Publications website at DOI: 10.1021/acsami.6b12779.

Drawing of PDMS curing mechanism and water-drop impinge test for steady porous silica structure; SEM images; SEM images indicating the stability of the superhydrophobicity against pH 3, 7, and 11 water and the preserved morphology of a damaged surface annealed at 500 °C; correlations between SCAs and the volume fraction of ethanol, propyl alcohol, and isopropanol; surface tension concentration dependence of ethanol−water mixtures; surface tension-responsive wettability of diverse surfaces; and role of the groove structure in generating particular wetting responsiveness on the AC-silica surface (PDF)

Video showing dyed water droplets bouncing off upon contacting the target surfaces (AVI)

Video showing the correlation between times and the SCA of the ethanol−water mixture ($V_e \approx 36\%$) on the BC-silica surface (AVI)

■ AUTHOR INFORMATION

Corresponding Author

*E-mail: zsguan@njtech.edu.cn. Tel: +86 025 83587270.

ORCID

Zisheng Guan: 0000-0002-5383-3626

Notes

The authors declare no competing financial interest.

■ ACKNOWLEDGMENTS

This work was funded by the National Natural Science Foundation of China (Grant 21071081). We also appreciate the lab support of the Collaborative Innovation Center for the Jangsu Advanced Inorganic Function Composite.

■ REFERENCES

(1) Barthlott, W.; Neinhuis, C. Purity of the Sacred Lotus, or Escape from Contamination in Biological Surfaces. *Planta* **1997**, *202*, 1−8.

(2) Sun, T. L.; Feng, L.; Gao, X. F.; Jiang, L. Bioinspired Surfaces with Special Wettability. *Acc. Chem. Res.* **2005**, *38*, 644−652.

(3) Li, X. M.; Reinhoudt, D.; Crego-Calama, M. What do We Need for a Superhydrophobic Surface? A Review on the Recent Progress in the Preparation of Superhydrophobic Surfaces. *Chem. Soc. Rev.* **2007**, *36*, 1350−1368.

(4) Feng, X. J.; Jiang, L. Design and Creation of Superwetting/Antiwetting Surfaces. *Adv. Mater.* **2006**, *18*, 3063−3078.

(5) Wen, L. P.; Tian, Y.; Jiang, L. Bioinspired Super-Wettability from Fundamental Research to Practical Applications. *Angew. Chem., Int. Ed.* **2015**, *54*, 3387−3399.

(6) Wang, S. T.; Liu, H. J.; Liu, D. S.; Ma, X. Y.; Fang, X. H.; Jiang, L. Enthalpy-Driven Three-State Switching of a Superhydrophilic/Superhydrophobic Surface. *Angew. Chem., Int. Ed.* **2007**, *46*, 3915−3917.

(7) Erbil, H. Y.; Demirel, A. L.; Avci, Y.; Mert, O. Transformation of a Simple Plastic into a Superhydrophobic Surface. *Science* **2003**, *299*, 1377−1380.

(8) Xie, Q. D.; Xu, J.; Feng, L.; Jiang, L.; Tang, W. H.; Luo, X. D.; Han, C. C. Facile Creation of a Super-Amphiphobic Coating Surface with Bionic Microstructure. *Adv. Mater.* **2004**, *16*, 302−305.

(9) Liu, Y.; Wang, X. W.; Fei, B.; Hu, H. W.; Lai, C. L.; Xin, J. H. Bioinspired, Stimuli-Responsive, Multifunctional Superhydrophobic Surface with Directional Wetting, Adhesion, and Transport of Water. *Adv. Funct. Mater.* **2015**, *25*, 5047−5056.

(10) Xin, B. W.; Hao, J. C. Reversibly Switchable Wettability. *Chem. Soc. Rev.* **2010**, *39*, 769−782.

(11) Huang, X.; Sun, Y. J.; Soh, S. Stimuli-Responsive Surfaces for Tunable and Reversible Control of Wettability. *Adv. Mater.* **2015**, *27*, 4062−4068.

(12) Burgess, I. B.; Mishchenko, L.; Hatton, B. D.; Kolle, M.; Loncar, M.; Aizenberg, J. Encoding Complex Wettability Patterns in Chemically Functionalized 3D Photonic Crystals. *J. Am. Chem. Soc.* **2011**, *133*, 12430−12432.

(13) Mishra, H.; Schrader, A. M.; Lee, D. W.; Gallo, A.; Chen, S. Y.; Kaufman, Y.; Das, S.; Israelachvili, J. N. Time-Dependent Wetting Behavior of PDMS Surfaces with Bioinspired, Hierarchical Structures. *ACS Appl. Mater. Interfaces* **2016**, *8*, 8168−8174.

(14) Lai, Y.; Gao, X.; Zhuang, H.; Huang, J.; Lin, C.; Jiang, L. Designing Superhydrophobic Porous Nanostructures with Tunable Water Adhesion. *Adv. Mater.* **2009**, *21*, 3799−3803.

(15) Wang, H.; Zhou, H.; Yang, W.; Zhao, Y.; Fang, J.; Lin, T. Selective, Spontaneous One-Way Oil-Transport Fabrics and Their Novel Use for Gauging Liquid Surface Tension. *ACS Appl. Mater. Interfaces* **2015**, *7*, 22874−22880.

(16) Vazquez, G.; Alvarez, E.; Navaza, J. M. Surface Tension of Alcohol + Water from 20 to 50.Degree.C. *J. Chem. Eng. Data* **1995**, *40*, 611−614.

(17) Meng, X. S.; Wang, Y.; Wang, H. N.; Zhong, J.; Chen, R. Y. Preparation of the Multifunctional Antireflective Films from a Templating Composite Silica Sol with Entwining Structures. *Surf. Coat. Technol.* **2013**, *236*, 518−524.

(18) Chen, Z.; Liu, X.; Wang, Y.; Li, J.; Guan, Z. Highly Transparent, Stable, and Superhydrophobic Coatings Based on Gradient Structure Design and Fast Regeneration from Physical Damage. *Appl. Surf. Sci.* **2015**, *359*, 826−833.

(19) Dyett, B. P.; Wu, A. H.; Lamb, R. N. Mechanical Stability of Surface Architecture−Consequences for Superhydrophobicity. *ACS Appl. Mater. Interfaces* **2014**, *6*, 18380−18394.

(20) Zhang, X.; Shi, F.; Niu, J.; Jiang, Y. G.; Wang, Z. Q. Superhydrophobic Surfaces: from Structural Control to Functional Application. *J. Mater. Chem.* **2008**, *18*, 621−633.

(21) Liu, X.; Wang, Y.; Chen, Z.; Ben, K.; Guan, Z. A Self-Modification Approach toward Transparent Superhydrophobic Glass for Rainproofing and Superhydrophobic Fiberglass Mesh for Oil−Water Separation. *Appl. Surf. Sci.* **2016**, *360*, 789−797.

(22) Liu, X.; Xu, Y.; Ben, K.; Chen, Z.; Wang, Y.; Guan, Z. Transparent, Durable and Thermally Stable PDMS-Derived Superhydrophobic Surfaces. *Appl. Surf. Sci.* **2015**, *339*, 94−101.

(23) Liu, X.; Xu, Y.; Chen, Z.; Ben, K.; Guan, Z. Robust and Antireflective Superhydrophobic Surfaces Prepared by CVD of Cured Polydimethylsiloxane with Candle Soot as a Template. *RSC Adv.* **2015**, *5*, 1315−1318.

(24) Vincent, A.; Babu, S.; Brinley, E.; Karakoti, A.; Deshpande, S.; Seal, S. Role of Catalyst on Refractive Index Tunability of Porous Silica Antireflective Coatings by Sol-Gel Technique. *J. Phys. Chem. C* **2007**, *111*, 8291−8298.

(25) Camino, G.; Lomakin, S. M.; Lazzari, M. Polydimethylsiloxane Thermal Degradation - Part 1. Kinetic Aspects. *Polymer* **2001**, *42*, 2395−2402.

DOI: 10.1021/acsami.6b12779
ACS Appl. Mater. Interfaces 2017, 9, 4142−4150

(26) Chen, Y.; Zhang, Y.; Shi, L.; Li, J.; Xin, Y.; Yang, T.; Guo, Z. Transparent Superhydrophobic/Superhydrophilic Coatings for Self-Cleaning and Anti-Fogging. *Appl. Phys. Lett.* **2012**, *101*, 033701.
(27) Bravo, J.; Zhai, L.; Wu, Z. Z.; Cohen, R. E.; Rubner, M. F. Transparent Superhydrophobic Films Based on Silica Nanoparticles. *Langmuir* **2007**, *23*, 7293−7298.
(28) Xiong, L.; Kendrick, L. L.; Heusser, H.; Webb, J. C.; Sparks, B. J.; Goetz, J. T.; Guo, W.; Stafford, C. M.; Blanton, M. D.; Nazarenko, S.; Patton, D. L. Spray-Deposition and Photopolymerization of Organic−Inorganic Thiol−ene Resins for Fabrication of Super-amphiphobic Surfaces. *ACS Appl. Mater. Interfaces* **2014**, *6*, 10763−10774.
(29) Zimmermann, J.; Artus, G. R. J.; Seeger, S. Long Term Studies on the Chemical Stability of a Superhydrophobic Silicone Nanofilament Coating. *Appl. Surf. Sci.* **2007**, *253*, 5972−5979.
(30) Christov, N. C.; Danov, K. D.; Kralchevsky, P. A.; Ananthapadmanabhan, K. P.; Lips, A. Maximum Bubble Pressure Method: Universal Surface Age and Transport Mechanisms in Surfactant Solutions. *Langmuir* **2006**, *22*, 7528−7542.
(31) Boreyko, J. B.; Baker, C. H.; Poley, C. R.; Chen, C. H. Wetting and Dewetting Transitions on Hierarchical Superhydrophobic Surfaces. *Langmuir* **2011**, *27*, 7502−7509.
(32) Koch, B. M. L.; Amirfazli, A.; Elliott, J. A. W. Wetting of Rough Surfaces by a Low Surface Tension Liquid. *J. Phys. Chem. C* **2014**, *118*, 23777−23782.
(33) Li, F.; Du, M.; Zheng, Q. Dopamine/Silica Nanoparticle Assembled, Microscale Porous Structure for Versatile Superamphiphobic Coating. *ACS Nano* **2016**, *10*, 2910−2921.
(34) Lee, C.; Kim, C. J. Maximizing the Giant Liquid Slip on Superhydrophobic Microstructures by Nanostructuring Their Sidewalls. *Langmuir* **2009**, *25*, 12812−12818.
(35) Hu, Z.; Zhang, X.; Liu, Z.; Huo, K.; Chu, P. K.; Zhai, J.; Jiang, L. Regulating Water Adhesion on Superhydrophobic TiO_2 Nanotube Arrays. *Adv. Funct. Mater.* **2014**, *24*, 6381−6388.
(36) Gao, X. F.; Yao, X.; Jiang, L. Effects of Rugged Nanoprotrusions on the Surface Hydrophobicity and Water Adhesion of Anisotropic Micropatterns. *Langmuir* **2007**, *23*, 4886−4891.

DOI: 10.1021/acsami.6b12779
ACS Appl. Mater. Interfaces 2017, 9, 4142−4150